Nanoscale

Cite this: *Nanoscale*, 2011, **3**, 4567

www.rsc.org/nanoscale

COMMUNICATION

Controllable formation and TEM spatial visualization of cross-linked gold nanoparticle spherical aggregates†

Guangyao Lin,[a] Yong Wang,[a] Qianjun Zhang,[a] Xiaoxiang Zhang,[a] Gang Ji[b] and Long Ba*[a]

Received 21st July 2011, Accepted 5th September 2011
DOI: 10.1039/c1nr10897b

Gold nanoparticles (NPs) were assembled and cross-linked into spherical aggregates by colloidal emulsion evaporation and ligand exchanging. The optical absorption, conventional transmission electron microscopy (TEM) and bright field (BF) TEM tomography confirm that the cross-linking of the pre-condensed aggregates generates high stability and compactness.

Motivated by the idea of generating new collective properties from the unique properties of individual nanoparticles (NPs) and their geometrical and chemical coupling, NPs have been assembled into superstructural blocks. The self-assembly of NPs can be a 2D monolayer or a 3D superlattice, which can be tuned by tailing the interaction between NPs.[1,2] Besides constructing ordered NP lattices, it is also interesting to assemble NPs into aggregates with regular shape. These NP aggregates can be fabricated *via* various mechanisms, such as molecular recognition through hydrogen bonding,[3] multidentate thioethers' cross-linking,[4–6] and electrostatic binding.[7] To further assemble NPs into blocks of regular shape with tunable and near equal interparticle chemical environment, several efforts have been made to bind NPs into stable submicrometre spherical aggregates.[8,9] The glue molecules can be as small as hundreds of Daltons which act as surface stabilizing and binding ligands. These monolayer interparticle ligands provide a new possibility to bind NPs into uniform aggregates within which the interparticle electronic state is almost equal, thus the hybrid aggregates can act as supermolecules with less property fluctuations. Unfortunately, few of the previous practices of bonding NPs into a regular superstructure have proven to be either stable in a solvent or linked by functional molecules.

The electron transportation through aromatic dithiols, which act as functional elements, has been calculated using density functional theory,[10,11] and measured using scanning probe microscopy on the planar deposited monolayer[12] and a dimer structure technique[13] for single molecule electronic devices. Recently, a report reveals that the cross-linking efficiency of aromatic dithiol is 4 times higher than aliphatic dithiol between CdTe quantum dots due to its rigid difference.[14] Though the simple alkanedithiol molecules can bridge NPs into spherical aggregates in monophase[4–6,8] or in emulsion,[9] the size uniformity and structure stability are still uncontrollable. Assembling gold NPs into monodisperse high symmetry blocks with a molecule like biphenyldithiol acting as both binding and electronic or photoelectronic functioning elements provides a promising strategy for the repeatable construction of molecular electronic devices. Using an emulsion evaporation technique, the monodisperse polymer spheres[15] and polydisperse NP aggregation spheres[7] can be fabricated. Because gold NPs passivated by alkanethiol have very weak interparticle interaction within a nonpolar solvent, the NPs can aggregate into spheres with tunable size by varying the concentration of NP colloidal solution and the droplet size of emulsion through a solvent evaporation process. Thus, it is possible to fabricate gold NP spherical aggregates through emulsion evaporation, ligand exchanging and cross-linking. Here we report our experimental study on the construction and the structure analysis of the sub-micrometre spherical aggregates. The microstructure of the spherical aggregates was analyzed by either conventional transmission electron microscopy (TEM) or bright field (BF) TEM tomography, which has been used to present the spatial structure with nanometre resolution for materials like viruses, NPs and nanovoids using three-dimensional (3D) reconstruction[16–19] during the last decade.

Gold NPs were fabricated by a two-phase liquid–liquid routine.[20] The dodecanethiol was used as a surface passivation molecule. To generate spherical aggregation by surface tension, we dropped 0.2 ml NP colloidal solution with concentration of about 1 mg ml^{-1} into 10 ml water, in which 1% w/v polyvinyl alcohol (PVA) ($M_w \approx 6000$) was dissolved. The chloroform phase was broken into emulsion using ultrasonic vibration. The stable emulsion was put into a vacuum rotary dryer to evaporate the colloidal droplets into solid aggregates. After 30 min evaporation in vacuum of about 100 mba at room temperature, the condensed aggregates in water were collected by centrifugation. To cross-link the gold NPs, octanedithiols or biphenyldithiols were dissolved in methanol with concentration of 0.2 mM. 5 ml 1 : 1 v/v methanol/water solution was used to dissolve the aggregates and the temperature was kept at 60 °C for 12 h. The cross-linked aggregates were collected by centrifugation. The morphology of NPs and their aggregates was analyzed using a Jeol 2100 TEM. The optical absorption spectra of dispersed Au NPs in chloroform, condensed aggregates in water, and cross-linked aggregates in

[a]*State Key Laboratory of Bioelectronics, School of Biology and Medical Engineering, Department of Physics, Southeast University, Nanjing, 210096, People's Republic of China.* Corresponding Author. E-mail: balong@seu.edu.cn; Fax: +86 25 83790951; Tel: +86 25 83790951*
[b]*Institute of Biophysics, Chinese Academy of Science, Beijing, 100201, People's Republic of China. E-mail: jigang@moon.ibp.ac.cn; Fax: +86 10 64871293; Tel: +86 10 64888419*

† Electronic supplementary information (ESI) available. See DOI: 10.1039/c1nr10897b

methanol were measured using a Shimadzu UV-3600 spectrometer. The BF TEM images with different tilt angles were recorded using a Gatan 894 CCD on a FEI TECNAI G2 microscope through FEI Xplore 3D tomography software suite. The image acquired was taken using automatic cross-correlation shift tracking and focused under dosage of 10e $Å^{-2} \cdot s^{-1}$. One frame was taken with exposure time of 0.5 s and the total 60 frames from −60° to +60° with 2° step were taken for about 30 min.

The size of as-prepared Au NPs scatters from 1 nm to 5 nm. The colloid monodispersity when dissolved within chloroform was demonstrated by both the optical absorption spectrum and the TEM image (Fig. S1 of the ESI†). The close packed hexagonal array of nanodots with nearly equal spacing distance demonstrates that the nonpolar solvent enables the very weak interparticle attraction within solution. The spherical aggregates were condensed from emulsion of colloidal solution in water. The chloroform phase was broken into disperse droplets using ultrasonic vibration. The NPs in the droplets were condensed into spherical aggregates by interfacial tension. The TEM image of the aggregates shows that most of the condensed spheres collapse into monolayer discs (Fig. 1a), which means that the aggregates are not stable without interparticle cross-link bonding. The inset, selected region electron diffraction (SAED) pattern, shows the typical nanocrystalline feature.

To enhance the interparticle adhesion stability, octanedithiol and biphenyldithiol were used as cross-linking molecules. Dithiol molecules exchange dodecanethiol bonded to the gold NP surface. Two –SH groups on the ends of one dithiol molecule provide anchor force to eliminate the slip mobility of the neighboring particles in the aggregates. To cross-link neighboring NPs, the aggregates were added to dithiol dissolved methanol/water solution. The mixture of methanol and water does not dissolve the hydrophobic aggregates. The compactness of the cross-linked aggregates can be enhanced by the evaporation of methanol during the cross-linking process. The TEM images (Fig. 1b and c) show that most of the aggregates keep circular shape. By tilting the sample to higher projection angle, it can be seen that most of the aggregates keep 3D structure. This means that the covalent bonds through dithiol molecules anchor the neighboring gold NPs from shear slip during drying on a substrate. The spacing distances between NPs are almost 1 nm, corresponding to the molecular length of the dithiols. To visualize the spatial structure of the aggregates, we have recorded a series of planar projection images for a typical sphere at different tilt angles.

The efficiency of the cross-linking was proved by optical absorption. Fig. 2 shows the surface plasmon resonance absorption of dispersed Au NPs and their aggregates. The concentration of NPs in chloroform is 1/5 of that of condensed and cross-linked samples. The red-shift of the resonance peak can be observed for the aggregates without cross-linking (Fig. 2, plot 2).

After adding dithiols, the optical absorption spectra of the samples cross-linked by octanedithiol or biphenyldithiol have no obvious peaks. The red-shift of the resonance peak was explained by the near-field coupling.[21] From our observation, the variation of the resonance peak from 524 nm of the dispersed NP to 578 nm of aggregates without cross-linking appears to be compatible with the systemic observation on the Au NP assemblies meditated by methylthio arylethynes,[22] while the optical absorption spectra measured on the cross-linked NPs show that the plasmon resonance is much depressed (very weak peak at 600 nm for the sample cross-linked by biphenyldithiols and almost no peak for the sample cross-linked by octanedithiols). The red-shift of the Au NPs in 2D closest packed configuration[1] or disordered multilayer thin film of Au NPs with

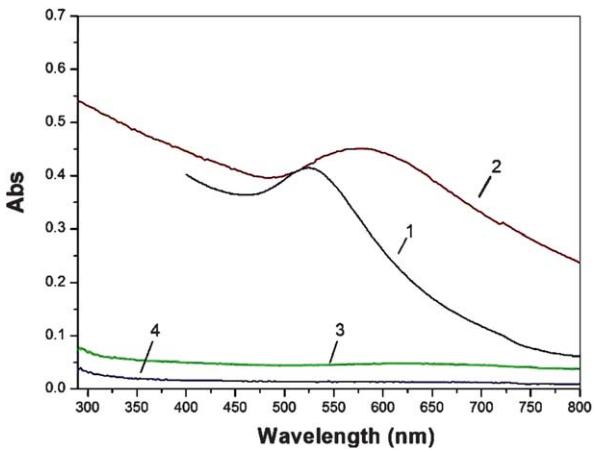

Fig. 2 Optical absorption of the NPs dissolved in chloroform (plot 1), aggregates condensed from emulsion evaporation (plot 2), cross-linked aggregates by biphenyldithiols (plot 3) and octanedithiols (plot 4).

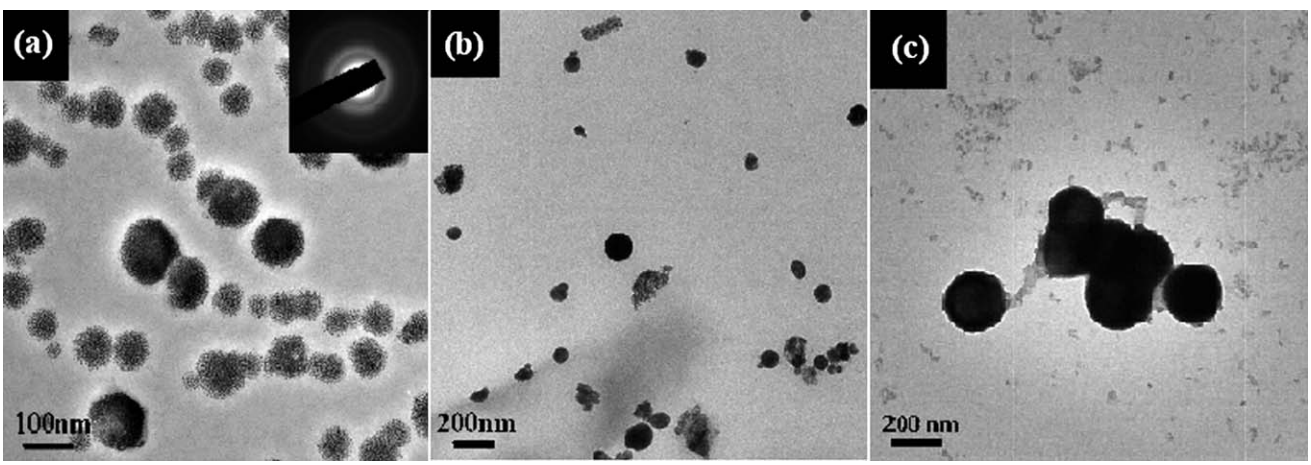

Fig. 1 TEM images of gold NP aggregates without cross-linking (a) (inset is a SAED pattern), cross-linked by octanedithiols (b) and cross-linked by biphenyldithiols (c).

alkanethiols of different chainlengths[23] was explained based on the Maxwell–Garnett formalism. But the decreased interparticle distance does not largely quench the plasmon resonance. Since the covalent bonding can lower the tunneling barrier and the electron transportation through Au electrodes is enhanced by dithiols,[24,25] it can be deduced that the loss of surface plasmon resonance may be caused by the higher electron transferring rate through neighboring NPs. The detailed mechanism needs further understanding.

Fig. 3 shows the aggregates cross-linked by octanedithiol or biphenyldithiol at various tilt angles. Though the 200 kV electron beam will unavoidably cause the evaporation of molecule residues and the ripening of gold NPs under continuous exposure to electron beam, there are no morphology changes on either the residual dithiol layer enveloped on the sphere or the particle size during our image acquiring process under careful dosage control.

Referring to the TEM images of the spherical aggregates of gold NPs cross-linked by multidentate thioethers[4] and alkanedithiols,[7] it can be seen that both molecules cannot provide enough stability and rigidity for the aggregates. The formation of the aggregates happened during the mixing of cross-linking molecules with surface passivated NPs in monophase solution or in biphase emulsion. Thus there are large irregular bonded NP clusters during ligand exchanging and cross-linking. The symmetry of the aggregates is deteriorated. Our strategy avoids this drawback. Before introducing cross-linking molecules, the shape of the condensates was controlled by the interfacial tension between chloroform and water. The high symmetry of the aggregates from our observation proves that the interfacial tension is strong enough to drive the weak interacted NPs into perfect spheres. The weak interaction between alkanethiol passivated gold NPs in nonpolar solvent not only enables the high monodispersity which reduces the aggregation within the solvent and thus increases the symmetry of the condensed spheres, but also enhances shear mobility of the condensed NPs under the interfacial tension during the solvent evaporation process, which can be seen from the near 2D discs of the NPs when dipping a drop of water containing NP condensates onto a copper grid (Fig. 1a).

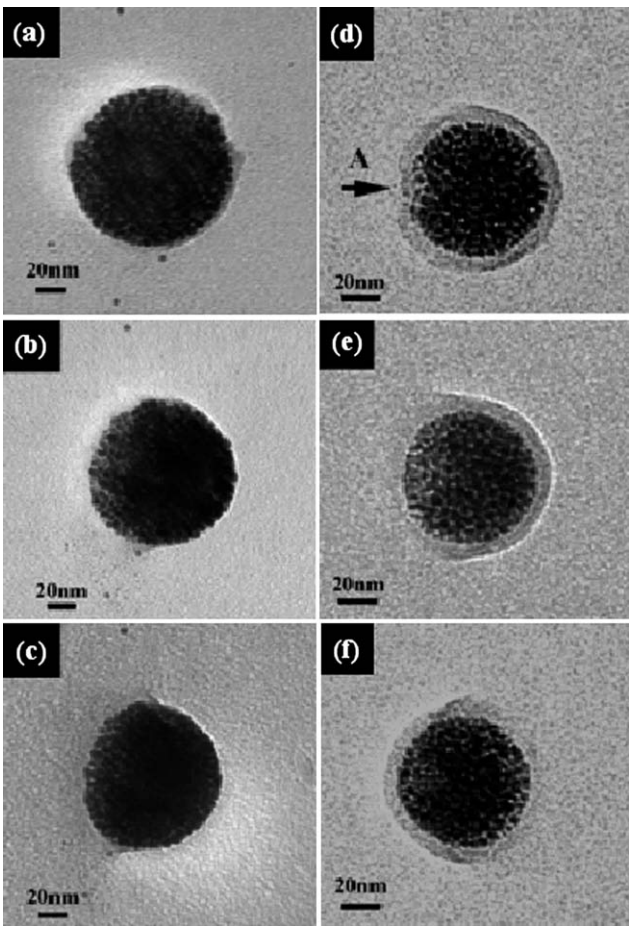

Fig. 3 TEM images of a typical spherical aggregate with different tilt angles and cross-linking molecules, (a) 0°, octanedithiol, (b) +45°, octanedithiol, (c) +63.8°, octanedithiol, (d) 0°, biphenyldithiol, (e) −45°, biphenyldithiol and (f) +60°, biphenyldithiol.

Octanedithiols and biphenyldithiols can stabilize the spheres through covalent cross-linking. But the efficiency of ligand exchange and cross-linking between these two molecules differs obviously. Measured from the TEM images of two typical spheres, the aspect ratio of the projection image at tilt angle of 63.8° for the sphere cross-linked by octanedithiols is about 0.916 (Fig. 3c), while that at 60° for the sphere cross-linked by biphenyldithiols is about 0.998 (Fig. 3f). The near 1 aspect ratio means that the contact angle between the sphere and substrate is near 0°. Based on a simple geometry model of sphere segment, the contact angle (~80°) can be calculated from the aspect ratio of different tilt angles for the sphere cross-linked by octanedithiol (Fig. 3a–c). Using our ligand exchanging and cross-linking strategy, the mixture of biphenyldithiol dissolved methanol and water presents sufficient interfacial tension which keeps the stability of the spherical aggregates due to the high polarity of the methanol/water mixture. The higher affinity of the methanol than water to the hydrophobic alkanethiol passivated NPs may enable the partial phase separation of methanol within the condensates. From our TEM observation of the sample cross-linked at room temperature and the reported images in ref. 7, most of the aggregates condensed from solvent evaporation and cross-linked by dithiols show plicate features like dried and folded capsules. This morphology can be explained by the evaporation of the trapped solvent within aggregates during ligand exchanging and cross-linking processes. The solvent residue thus relaxes the close contact between neighboring hydrophobic NPs and decreases the cross-linking efficiency within aggregates. By elevating the cross-linking temperature, the methanol was evaporated and most of the dithiols were carried out of the aggregates. This largely reduces the volume of solvent and dithiol residues and unanchored NPs within the sphere. The much larger contact angle of the sphere cross-linked by octanedithiols confirms that the cross-linking efficiency of flexible alkanedithiols does not give enough rigidity between neighboring NPs.

The compactness of the aggregates can be visualized from 3D images reconstructed and displayed using software of Inspect3D. Fig. 4 shows the reconstructed 3D rendering of the sphere at 0° and 45° viewing orientation. The tilting axial is indicated as *y* in the view plane. Though the finite tilt angles of TEM tomography cause some distortion of the NPs on the reconstructed image, the spatial configuration of the NPs can be clearly identified in the 3D image. Its near perfect spherical shape with a diameter of about 68 nm was confirmed. By generating an isosurface image, the individual NP and gap between neighboring NPs can be identified. The less compact region within the sphere (labelled as A in Fig. 3d and 4a) clearly indicates that there is molecular residue trapped in the sphere. In this region the inter-particle distance is much larger than 1 nm, which is

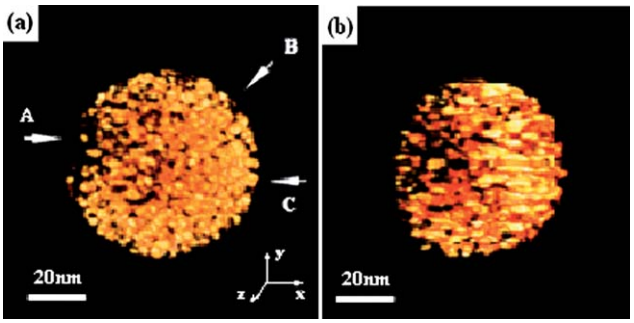

Fig. 4 3D reconstructed isosurface rendering viewing at 0° (a) and 40° (b) for the sphere as shown in the BF image of Fig. 3(d–f).

more obvious viewing at 45° (Fig. 3b). It shows that the left part of the sphere traps more dithiols than the right part. From the reconstructed image, the shape and size of the particles and interparticle voids are unavoidably distorted by the missing wedges of the TEM tomography. On the surface, the resolution of the isolated particle and gap can reach 1 nm (labelled as B in Fig. 4a). The distortion can cause the margin of some particles cannot be clearly depicted (labelled as C in Fig. 4a). Despite a few uncertainties, the spatial position of most of the NPs within the aggregate can be identified through 3D reconstruction with nanometre resolution.

In summary, we have demonstrated the formation of gold NP nanospherical aggregates through ligand exchanging and molecular monolayer cross-linking under controllable conditions. TEM and TEM tomography show that the spherical aggregates cross-linked by a rigid biphenyldithiol monolayer are more stable than the aggregates cross-linked by a flexible octanedithiol monolayer. 3D reconstruction demonstrates that the spatial configuration of an individual NP can be visualized with nanometre resolution. This spatial visualization confirms that the stability of the spherical aggregates relies on the effective cross-linking between neighboring NPs.

Acknowledgements

This work is supported by the Natural Science Foundation of China under grant no. 10774022 and Jiansu Provincial Social Development Program under grant no. BE2009665.

References

1 J. R. Heath, C. M. Knobler and D. V. Leff, *J. Phys. Chem. B*, 1997, **101**, 189–197.
2 W. H. Evers, B. D. Nijs, L. Filion, S. Castillo, M. Dijkstra and D. Vanmaekelbergh, *Nano Lett.*, 2010, **10**, 4235–4241.
3 A. K. Boal, F. Ilhan, J. E. DeRouchey, T. Thurn-Albrecht, T. P. Russell and V. M. Rotello, *Nature*, 2000, **404**, 746–748.
4 M. M. Maye, S. C. Chun, L. Han, D. Rabinovich and C. J. Zhong, *J. Am. Chem. Soc.*, 2002, **124**, 4958–4959.
5 M. M. Maye, J. Luo, I. I. S. Lim, L. Han, N. N. Kariuki, D. Rabinovich, T. B. Liu and C. J. Zhong, *J. Am. Chem. Soc.*, 2003, **125**, 9906–9907.
6 M. M. Maye, I. I. S. Lim, J. Luo, Z. Rab, D. Rabinovich, T. B. Liu and C. J. Zhong, *J. Am. Chem. Soc.*, 2005, **127**, 1519–1529.
7 F. Bai, D. Wang, Z. Huo, W. Chen, L. Liu, X. Liang, C. Chen, X. Wang, Q. Peng and Y. Li, *Angew. Chem., Int. Ed.*, 2007, **46**, 6650–6653.
8 I. Hussain, Z. Wang, M. Brust and A. I. Cooper, *Langmuir*, 2006, **22**, 2938–2941.
9 I. Hussain, H. Zhang, M. Brust, J. Barauskas and A. Cooper, *J. Colloid Interface Sci.*, 2010, **350**, 368–372.
10 R. Cohen, K. Stokbro, J. M. L. Martin and M. A. Ratner, *J. Phys. Chem. C*, 2007, **111**, 14893–14902.
11 H. Kondo, J. Nara, H. Kindo and T. Ohno, *J. Chem. Phys.*, 2008, **128**, 064701.
12 A. Mishchenko, D. Vonlanthen, V. Meded, M. Bürkle, C. Li, I. V. Pobelov, A. Bagrets, J. K. Viljas, F. Pauly, F. Evers, M. Mayer and T. Wandlowski, *Nano Lett.*, 2010, **10**, 156–163.
13 T. Dadosh, Y. Gordin, R. Krahne, I. Khivrich, D. Mahalu, V. Frydman, J. Spering, A. Yacoby and I. Bar-Joseph, *Nature*, 2005, **436**, 677–680.
14 R. Koole, B. Luigjes, M. Tachiya, R. Pool, T. J. H. Vlugt, C. D. M. Donega, A. Meijerink and D. Vanmaekelbergh, *J. Phys. Chem. C*, 2007, **111**, 11208–11215.
15 Q. Xu, M. Hashimoto, T. T. Dang, T. Hoare, D. S. Kohane, G. M. Whitesides, R. Langer and D. G. Anderson, *Small*, 2009, **5**, 1575–1581.
16 P. A. Midgley and M. Weyland, *Ultramicroscopy*, 2003, **96**, 413–431.
17 R. Sperling, A. J. Kroster, C. Melamed-Bessudo, A. Rubinstein, M. Angenitzki, Z. Berkovitch-Yellin and J. Sperling, *J. Mol. Biol.*, 1997, **267**, 570–583.
18 K. P. de Jong and A. I. Koster, *ChemPhysChem*, 2002, **3**, 776–780.
19 J. B. Park, J. H. Lee and H. R. Choi, *Appl. Phys. Lett.*, 2007, **90**, 093111.
20 M. Brust, M. Walker, D. Bethell, D. J. Schiffrin and R. Whyman, *J. Chem. Soc., Chem. Commun.*, 1994, 801.
21 W. Y. Huang, W. Qian, P. K. Jain and M. A. El-Sayed, *Nano Lett.*, 2007, **7**, 3227–3234.
22 H. Yan, S. I. Lim, L. C. Zhang, S. C. Gao, D. Mott, Y. Le, R. Loukrakpam, D. L. An and C. J. Zhong, *J. Mater. Chem.*, 2011, **21**, 1890–1901.
23 V. V. Agrawal, N. Varghese, G. U. Kulkani and C. N. R. Rao, *Langmuir*, 2008, **24**, 2494–2500.
24 X. D. Cui, A. Primak, X. Zarate, J. Tomfohr, O. F. Sankey, A. L. Moore, T. A. Moore, D. Gust, G. Harris and S. M. Lindsay, *Science*, 2001, **294**, 571–574.
25 E. Loertscher, C. J. Chao, M. Mayor, M. Tsuchudy, C. Rettner and H. Riel, *ChemPhysChem*, 2011, **12**, 1677–1682.

